PCCP

PAPER

Cite this: *Phys. Chem. Chem. Phys.*, 2017, **19**, 7359

Absorption behavior of poly(methyl methacrylate)–multiwalled carbon nanotube composites: effects of UV irradiation†

Je-Chuan Hsu,[a] Wenxin Cao,[b] Fuqian Yang,[b] Tsong-Jen Yang[c] and Sanboh Lee*[a]

Received 22nd December 2016,
Accepted 17th February 2017

DOI: 10.1039/c6cp08738h

rsc.li/pccp

Understanding the effects of carbon nanotubes (CNTs) and ultraviolet (UV) irradiation on solvent transport in polymers is of practical importance for the applications of polymer–CNT composites in electronics and photonics. The transport behavior of methanol in poly(methyl methacrylate)–multiwalled carbon nanotube (PMMA–MWCNT) composites with and without UV light irradiation has been studied. The anomalous transport has been investigated as a function of the weight percentage of MWCNTs and UV dose in the temperature range of 30–50 °C. The anomalous transport consists of Case I (controlled by concentration gradient) and Case II (controlled by stress relaxation) transport; both UV irradiation and the addition of MWCNTs in PMMA enhance the transport of methanol. The activation energies for Case I and Case II transport decrease with the increase of UV dose for the PMMA–MWCNT plates with the same weight percentage of MWCNTs. Without UV irradiation, the activation energy for Case I transport of methanol decreases with the increase of the weight percentage of MWCNTs, and the activation energy for Case II transport increases with the increase of the weight percentage of MWCNTs.

1. Introduction

Carbon nanotubes (CNTs) discovered first by Iijima in 1991[1] exhibit unique properties, including high elastic modulus, chemical stability, electrical conductivity, and high specific surface area. The combination of a high elastic modulus and a good response of CNTs to an electric field has made polymer/CNT-based nanocomposites promising materials for applications in sensing and actuating technologies.[2,3] One of the challenges in the applications of polymer/CNT-based nanocomposites is the swelling induced by the volume changes associated with the migration of ions within the porous structure formed by the carbon nanotubes[4–6] and the diffusion of solvents in the polymer matrix,[7–10] which can lead to a change in mechanical structures involving creep and stress relaxation and limit the applications of polymer/CNT-based nanocomposites.

Michardière *et al.*[11] formed composite CNT–PVA (poly(vinyl alcohol)) fibers and used PVA to reduce the stress relaxation likely associated with ionic swelling as observed in CNT yarns made from forests of multiwalled nanotubes (MWNTs).[12,13] Shah *et al.*[14] prepared CNT–hydrogel composites and demonstrated that the CNTs impeded the hydrogel crosslinking resulting in longer gelation times and higher swelling above a threshold CNT concentration. Abraham *et al.*[15] studied the effect of CNT concentration on the transport behavior of solvents in styrene butadiene rubber and found that the swelling index decreases upon increasing the CNT concentration irrespective of the solvent used. Starkova *et al.*[16] studied moisture and water uptake of epoxy/MWCNT composites, and noted the twofold decrease of the diffusivity with the addition of up to 1 wt% of MWCNTs into the neat epoxy. They suggested the presence of two types of water (“free” water and “bound” water”) in the materials and their different contributions to the transport properties of the epoxy/MWCNT composites. Kim *et al.*[17] studied the effect of seawater absorption on the damping and fracture behaviors of CNT-modified epoxy/basalt fiber (basalt/CNT/epoxy) multiscale composites and suggested that the decrease of the fracture toughness of the seawater-absorbed basalt/CNT/epoxy multiscale composites was due to the swelling of the epoxy matrix. Yu *et al.*[18] examined the tensile properties of polyisoprene–CNT composites and suggested that the restraining effect of CNTs on swelling in the composites provides reinforcement due to a tightly bound interfacial layer on the CNTs, which was augmented by cross-linking under high pressure conditions. Yip *et al.*[19] developed CNT–ionic polymer actuators and found that

[a] *Department of Materials Science and Engineering, National Tsing Hua University, Hsinchu 300, Taiwan. E-mail: sblee@mx.nthu.edu.tw; Fax: +886-3-5719677; Tel: +886-3-5719677*
[b] *Department of Chemical and Materials Engineering, University of Kentucky, Lexington, KY 40506, USA*
[c] *Department of Materials Science and Engineering, Feng-Chia University, Taichung, Taiwan*

† Electronic supplementary information (ESI) available. See DOI: 10.1039/c6cp08738h

a higher percentage of CNTs lowers the water absorption rate, and increases the constraint of the matrix to reduce swelling and deformation. Villmow *et al.*[20] prepared polycarbonate–CNT composites for liquid sensing and noted that a composite with a higher CNT content had a smaller resistance change than a composite of a smaller CNT amount due to the CNT-induced increase of the resistance to the diffusion of solvents. None of the studies has addressed the effect of UV (ultraviolet) light on the swelling of polymer–CNT composites.

UV light irradiation to polymers can cause a change in microstructures *via* the crosslinking polymerization[21] or the breakage of chemical bonds.[22] It is expected that the change in the microstructures of polymers due to UV irradiation will also lead to the change in the resistance to the diffusion of solvents and the associated swelling behavior. Considering the important applications of polymer–CNT composites in sensing and actuating technologies, we investigate the absorption behavior of poly(methyl methacrylate)–multiwalled carbon nanotube (PMMA–MWCNT) composites with and without UV light irradiation in methanol. The diffusivity of methanol in the PMMA–MWCNT composites is characterized, and the temperature dependence of the diffusivity is discussed.

2. Experimental details

Polymerization was used to prepare PMMA–MWCNT composites. A methyl methacrylate monomer (MMA-monomer) with a density of 0.94 g cm^{-3} was obtained from Kaohsiung Monomer Company (Taiwan), and MWCNTs with a purity of more than 95% and a specific surface area of 110 m^2 g^{-1} were obtained from Legend Star International Co., Ltd (New Taipei, Taiwan). The outer diameter and inner diameter of the MWCNTs were 20–30 nm and 5–10 nm, respectively, and the length of the MWCNTs was 10–30 μm. The solution of 20 g of the MMA-monomer and MWCNTs in a glass reactor was ultrasonically sonicated at 50 °C for 2 h in order to disperse the MWCNTs in the MMA monomer. After sonication, a few drops of polyethylene glycol octylphenyl (Triton X-100, ACROS ORGANICS, Geel, Belgium) as a surfactant was added into the solution, which was ultrasonically sonicated for 1.5 h, to improve the dispersion of MWCNTs. An aqueous solution with 0.025 wt% of the initiator, AIBN (2,2-azobisisobutylnitrile, AENCORE CHEMICAL, Surrey Hills, Victoria, Australia) was then added into the previous solution, and was ultrasonically sonicated for 1.5 h. After sonication, the final solution was placed in a Pyrex plate container and heated in a water bath for polymerization at 80 °C for 30 min. After the polymerization, the final solution became viscous, and was placed in a water bath at 40 °C for 24 h to achieve a fully polymerized state and form a PMMA–MWCNT composite. The formed PMMA–MWCNT composite was immersed in acetone and then washed with DI water to remove the residual reactants. Finally, the PMMA–MWCNT composite was dried in a vacuum oven at 90 °C to vaporize unreacted MMA monomers.

PMMA–MWCNT plates of 5 × 5 × 1 mm^3 were cut from the prepared PMMA–MWCNT composites. The plates were ground by emery papers of 400, 800, 1200, and 2000 grit and then polished by alumina slurries of 1 and 0.05 μm in sequence. The polished plates after being sonicated in DI water were heat-treated in air at 90 °C for 24 h to release the residual stresses introduced during the preparation processes.

The heat-treated plates were immersed in methanol in a glass beaker at a pre-set temperature in a water bath. The PMMA–MWCNT plates were periodically removed from methanol, and the weight gain was recorded until there was no weight change. An analytical balance (OHAUS – AP250D, Pine Brook, NJ) was used to measure the weight of the PMMA–MWCNT plates.

UV light irradiation was performed on the heat-treated PMMA–MWCNT plates in a drawer type UV curing machine with a high pressure mercury lamp of 1 kW (KINGO Electrical Enterprise Co., Tainan, Taiwan) and two filters ($\lambda > 300$ nm). An IR filter was used to maintain the specimen chamber at 37 °C during UV irradiation. The other filter was used to allow only UV light irradiation with wavelength less than or equal to 254 nm for various durations to achieve the desired doses of 291.87 and 583.74 J cm^{-2}, respectively. The irradiation rate of UV light was 1.15 mW cm^{-2}, as measured using a G&R Labs power meter (Santa Clara, CA).

The surface morphology of the PMMA–MWCNT plates was analyzed, using an atomic force microscope (AFM) in the tapping mode (Dimension Icon AFM microscope, Bruker, Santa Barbara, CA). The phase information, *i.e.* PMMA and CNTs, was determined from the phase shift due to the difference in the interaction between the AFM tip and the surface of materials.[23,24] The resonance frequency of the Si-based AFM tip is 330 kHz. The AFM images were analyzed by the Nanoscope Analysis software.

The Raman spectrum of the individual powder of PMMA and the PMMA–MWCNT composite was recorded at room temperature to analyze the chemical structures of PMMA and the PMMA–MWCNT composite, using LabRAM HR800 UV Confocal Micro-Raman Spectroscopy (Horiba, Ltd., Minami-Ku, Kyoto, Japan). Scanning was performed in the range of 700 to 3800 cm^{-1} using a high-power helium neon laser (λ = 632.8 nm) system.

3. Results and discussion

Surface morphology of PMMA–MWCNT composites

Fig. 1a and b show the SEM images of MWCNTs used in the preparation of the PMMA–MWCNT composites. As shown in the embedded SEM image in Fig. 1a, the ends of the MWCNTs are open. The open end of MWCNTs likely allows the flow/diffusion of solvents through the MWCNTs. The average outer diameter of the MWCNTs is ~19.5 nm, as calculated from the MWCNTs with labeled numbers in Fig. 1b. Fig. 1c–e show the SEM images of the fractured surfaces of the PMMA–MWCNT composites. One can note that the fraction of MWCNTs increases with the increase of the weight percentage of MWCNTs.

AFM was used to examine the uniformity of MWCNTs dispersed in the PMMA matrices. Fig. 2 shows the phase mode of the AFM images of the PMMA–MWCNT composites of 0.1 wt% MWCNTs with the prepared surfaces at different distances to

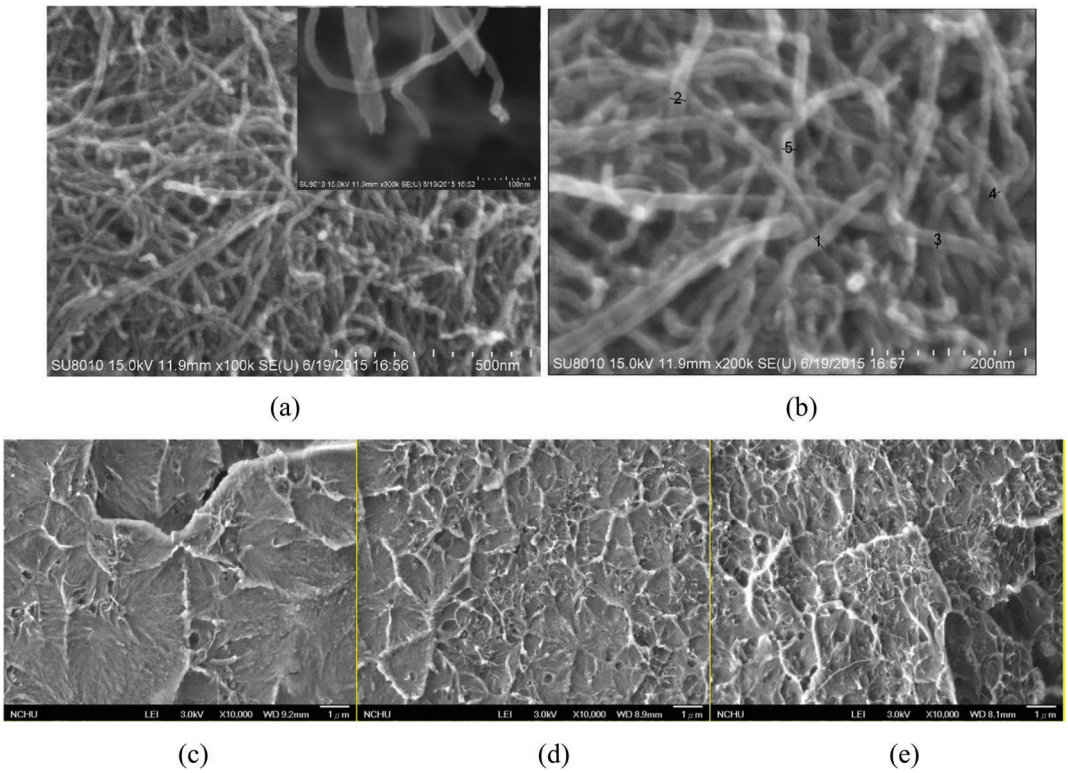

Fig. 1 SEM images of MWCNTs and the fractured surfaces of PMMA–MWCNT composites; (a) MWCNTs used in the preparation of the PMMA–MWCNT composites where the inset shows the open end of carbon nanotube, (b) MWCNTs labeled with numbers which were used to calculate the outer diameter of the MWCNTs, (c) PMMA–MWCNT composite with 0.1 wt% of MWCNTs, (d) PMMA–MWCNT composite with 0.4 wt% of MWCNTs, and (e) PMMA–MWCNT composite with 0.7 wt% of MWCNTs.

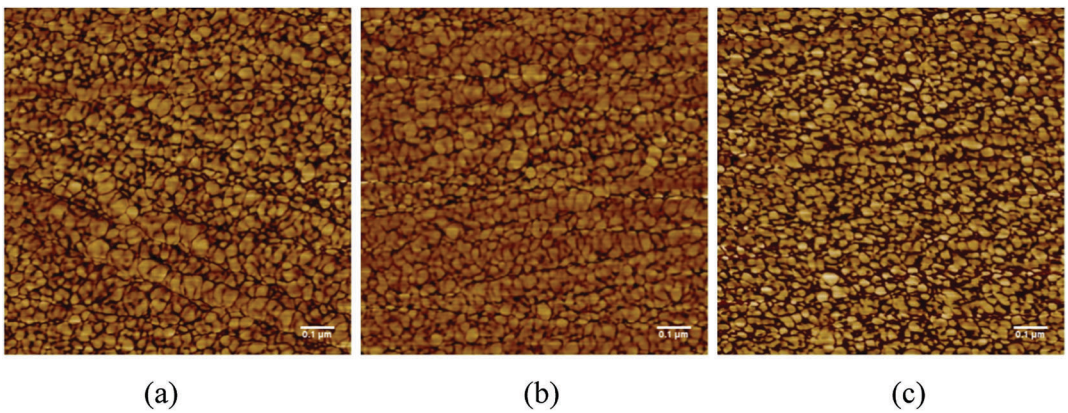

Fig. 2 AFM images of a PMMA–MWCNT composite of 0.1 wt% MWCNTs with the prepared surfaces at different distances to the initially free surface: (a) 0 mm, (b) 1 mm, and (c) 2 mm.

the initially free surface, in which the orientation of the MWCNTs varies between 0° (the length direction of MWCNTs is parallel to the surface of the PMMA matrix) and 90° (the length direction of MWCNTs is perpendicular to the surface of the PMMA matrix). There are bright and dark regions which arrange alternately. In the bright regions, the orientation of MWCNTs has large angles (around 90°) relative to the surface of the PMMA matrix. In the dark regions, there is deficiency of MWCNTs or the orientation of MWCNTs has small angles (around 0°) relative to the surface of the PMMA matrix. The distribution of the bright and dark regions is relatively uniform. There are only small changes over the local areas, no significant difference between the distributions of the bright and dark regions is observed for the PMMA–MWCNT composites at three different locations in the same specimen. This result suggests that the MWCNTs were dispersed relatively well in the PMMA–MWCNT composites.

Fig. 3 shows the comparison of the AFM images of the PMMA–MWCNT composites in the phase mode with and

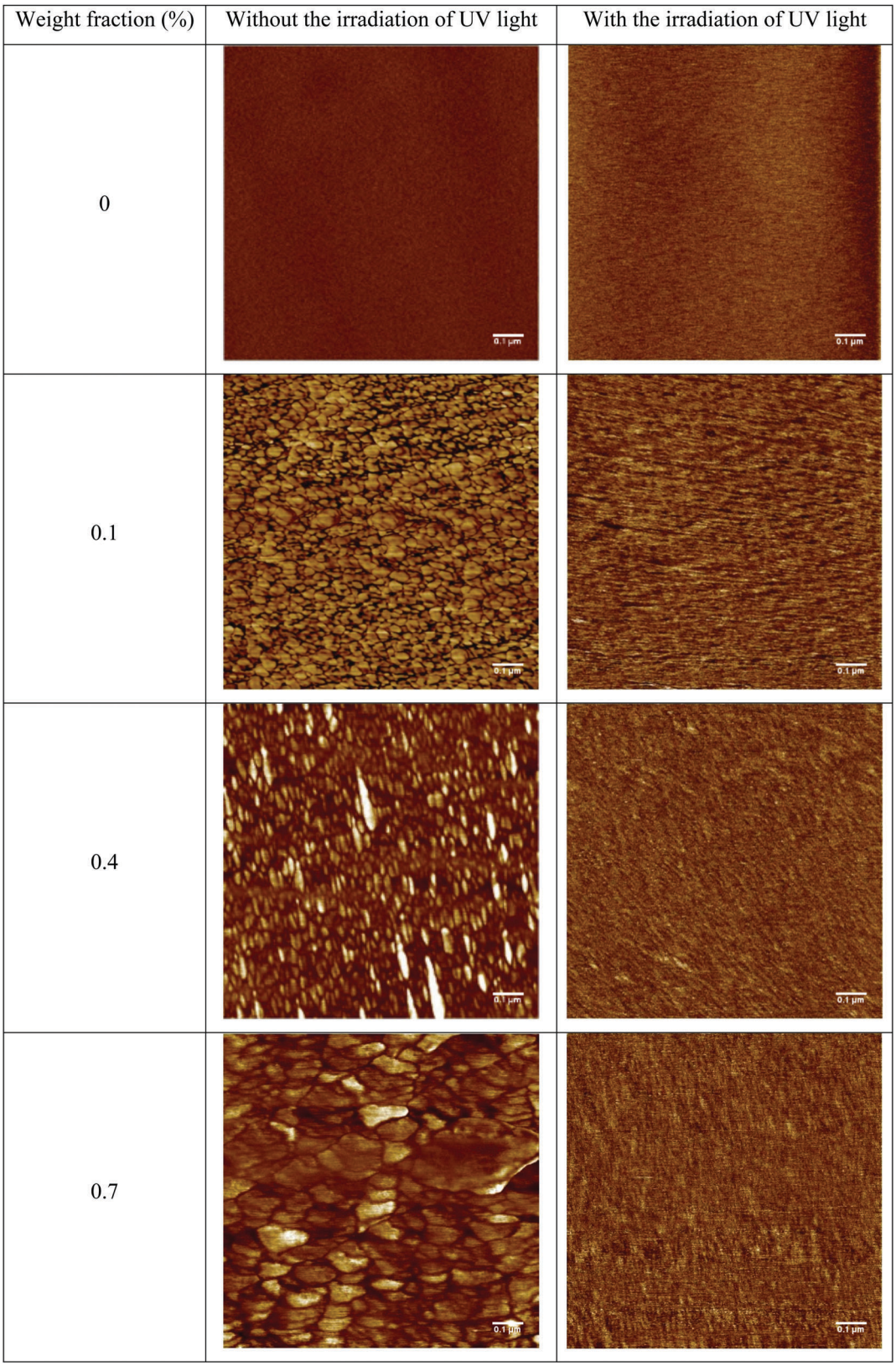

Fig. 3 Comparison of the AFM images of the PMMA–MWCNT composites in the phase mode with and without UV light irradiation for different weight fractions of MWCNTs.

Table 1 Surface roughness (R_q in the unit of nm) of the PMMA–MWCNT composites with different weight percentages of MWCNTs with and without UV irradiation

	MWCNT			
Dose	0 wt%	0.1 wt%	0.4 wt%	0.7 wt%
0 (J cm^{-2})	5.97	29.2	38.3	29.9
291.87 (J cm^{-2})	14.1	27.1	22.3	18.4

without UV light irradiation for different weight fractions of MWCNTs. It is evident that UV light irradiation caused a change in the surface morphologies of the PMMA–MWCNT composites due to the interaction between PMMA and UV light. No zones are associated with either the bright or dark region. The surfaces of the PMMA–MWCNT composites become smeared after UV light irradiation, while UV light irradiation did not cause any observable change on the surface of pure PMMA plates. Using Software ImageJ (National Institute of Health, Bethesda, MD), the surface roughness of the PMMA–MWCNT composites with and without UV light irradiation was measured.

Table 1 lists the surface roughness of the PMMA–MWCNT composites with different weight fractions of MWCNTs with and without UV irradiation. Without MWCNTs in PMMA, UV irradiation causes an increase of surface roughness. Such behavior is associated with the UV-induced chain scission, resulting in the formation of free ends of polymer chains on the free surface of PMMA, which was not under any constraint. For the same weight fraction of MWCNTs larger than or equal to 0.1%, the surface roughness of the PMMA–MWCNT composites with UV irradiation is always smaller than that without UV irradiation. Also, the surface roughness of the PMMA–MWCNT composites with UV irradiation decreases with the increase of the weight fraction of MWCNTs. These results reveal the constraint of MWCNTs on the motion of polymer chains and the strong interaction between PMMA and MWCNTs, even though UV irradiation causes chain scission. A dense, entangled PMMA–MWCNT layer was formed after UV irradiation.

Raman spectra of PMMA–MWCNT composites

Fig. 4 shows the Raman spectra of the PMMA–MWCNT composites with different weight fractions of MWCNTs. The D-band and G-band appear at 1335 cm^{-1} and 1581 cm^{-1}, respectively. Note that the D-band represents the disorder structure and the defect components in CNTs associated with unstable C–C bonds; the G-band represents the graphitic structure associated with stable C–C bonds. No new peak is present for the PMMA–MWCNT composites without UV irradiation, while there is new small peak at 1647 cm^{-1} for pure PMMA with UV irradiation. This peak can be attributed to the olefinic unsaturation produced during the photolytic chain scission. Unsaturated C=C bonds were formed from the ester side, resulting in chain cleavage or separation of the side chain from the carbonyl group. The intensities for the peaks at wave numbers of 1447 and 1728 cm^{-1} for PMMA slightly increase after UV light irradiation. Such a result suggests that photo-induced degradation of PMMA occurs,

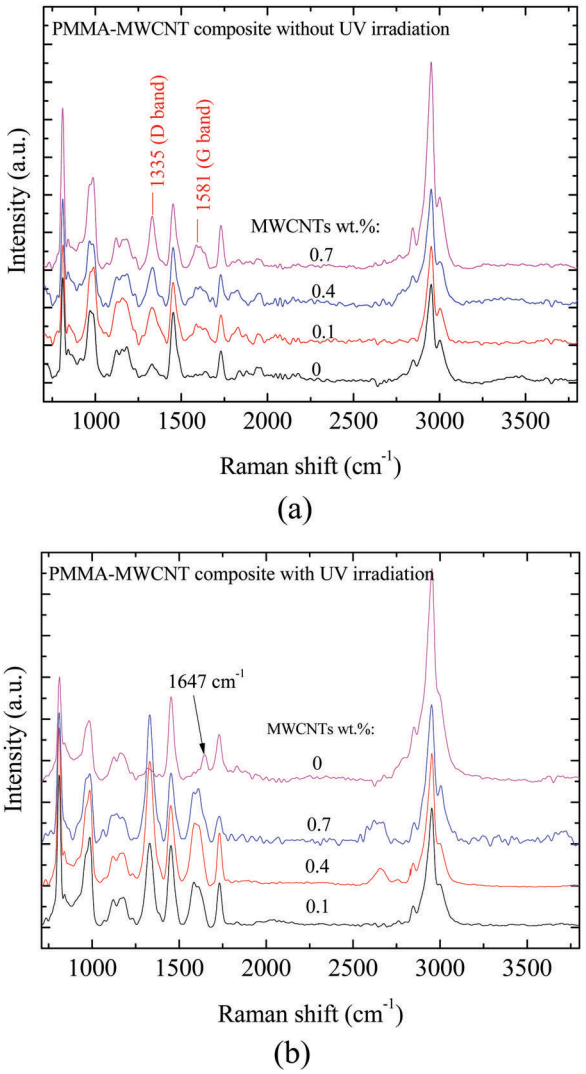

Fig. 4 Raman spectra of PMMA–MWCNT composites with different weight fractions of MWCNTs; (a) without UV irradiation, and (b) with UV irradiation of an irradiation dose of 291.87 J cm^{-2}.

which leads to the release of MMA to the environment during UV light irradiation.

The D–G band ratio (I_D/I_G), which is calculated as the ratio of the D-band intensity to the G-band intensity, has been used to analyze the concentration of defects in carbon nanotubes. Table 2 lists D–G band ratios for the PMMA–MWCNT composites with different weight fractions of MWCNTs with and without UV irradiation. For comparison, the D–G band ratio for the as-received MWCNTs is 1.34. The D–G band ratio increases with the increase of the weight fraction of MWCNTs, and all three PMMA–MWCNT composites have larger D–G band ratios than the as-received MWCNTs. This result suggests that the dispersion of MWCNTs in a PMMA matrix can lead to the increase of the defects in MWCNTs since the unstable C–C bonds become more reactive for the radical polymerization of methyl methacrylate initiated by AIBN to form stable C–C bonds. The increase of the D–G band ratio also reveals the trend that the difficulty of dispersing MWCNTs in PMMA increases with

Table 2 D–G band ratios for the PMMA–MWCNT composites with different weight fractions of MWCNTs and UV doses

	MWCNT			
Dose	0 wt%	0.1 wt%	0.4 wt%	0.7 wt%
0 (J cm^{-2})	1.05	1.80	1.90	2.15
291.87 (J cm^{-2})	2.09	1.85	1.64	1.55

the increase of the concentration of MWCNTs because of the increase of the defect concentration of MWCNTs. Note that UV irradiation caused a decrease of the D–G band ratio with the increase of the weight fraction of MWCNTs, suggesting that UV irradiation can reduce the defect concentration of MWCNTs. It has been reported that the initiator (AIBN) opens the π-bonds in the external walls of MWCNTs to produce an unstable Csp^3 dangling bond.[25] UV irradiation also led to partial degradation of PMMA *via* a free-radical chain reaction mechanism. The recombination of free radicals in MWCNTs and PMMA indicates strong interaction with the formation of stable C–C bonds.

Mass transport of methanol in PMMA–MWCNT composites

The mass transport of methanol in the PMMA–MWCNT composites was studied, using an analytical balance to measure the weight change of the PMMA–MWCNT plates, which were immersed in methanol. Fig. 5 shows the temporal variation of the mass ratio of methanol absorbed in the UV-irradiated PMMA–MWCNT composites to the equilibrium amount of methanol (M_t/M_∞) absorbed in the UV-irradiated PMMA–MWCNT composites, which were immersed in methanol at 50 °C. Here, M_t is the amount of methanol absorbed in the PMMA slab over an immersion time t, and M_∞ is the equilibrium amount of methanol absorbed in the slab as the immersion time approaches infinity. It is evident that both the irradiation dose and the weight fraction of MWCNTs play important roles in the absorption of methanol in the PMMA–MWCNT composites. The absorption rate of methanol into the PMMA–MWCNT composites decreases gradually with the immersion time. This trend is independent of UV irradiation and the weight percentage of MWCNTs. The time to achieve equilibrium absorption decreases with the increase of the weight fraction of MWCNTs in contrast to the result given by Yip *et al.*[19] that a higher percentage of CNTs lowers the water absorption rate. The MWCNTs enhance the diffusion of methanol in the PMMA–MWCNT plates.

According to the theory of anomalous mass transport,[26–31] the driving force for the diffusion of solvents to a polymer is controlled by the difference of solvent concentration and stress relaxation during the penetration of the solvents into the polymer. Adding MWCNTs in PMMA causes the reaction of a portion of the C–C bonds in MWCNTs to establish a linkage between MWCNTs and PMMA chains and leads to wrapping of some MWCNTs with PMMA chains. This result increases the free volume in the PMMA and causes the formation of the interface-phase between MWCNTs and PMMA, which reduces the resistance for the diffusion of methanol.

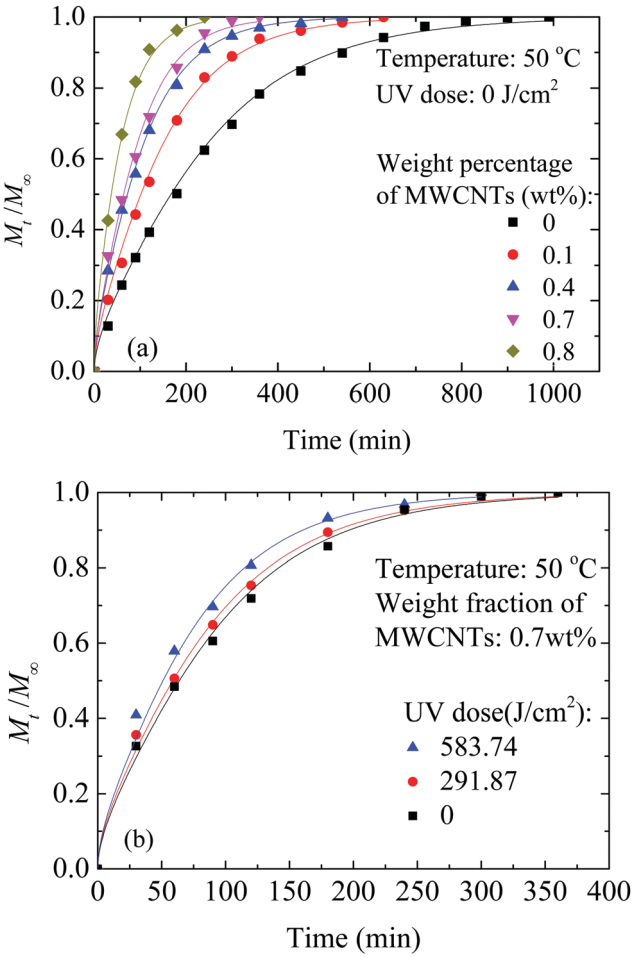

Fig. 5 Temporal variation of the mass ratio of methanol absorbed in the UV-irradiated PMMA–MWCNT composites to the equilibrium amount of methanol absorbed in the UV-irradiated PMMA–MWCNT composites immersed in methanol at 50 °C; (a) without UV irradiation for different weight percentages of MWCNTs, and (b) with a weight percentage of 0.7% MWCNTs for different UV doses.

From Fig. 5, one can note that the time to achieve the equilibrium absorption decreases with the increase of the irradiation dose for the PMMA–MWCNT composites with the same weight fraction of MWCNTs. Such a result is attributed to the UV-induced chain scission, which causes the slack of chain alignments and increases the free volume in PMMA. Methanol can diffuse into the UV-irradiated PMMA at a fast rate.

There are three categories for the transport behavior of solvents in polymers,[27] including Case I, Case II and anomalous transport. The Case I transport is Fickian diffusion, and the Case II transport is dominated by stress relaxation of polymer chains. Anomalous transport occurs when the effect of solvent penetration is comparable to the effect of stress relaxation. Harmon *et al.*[29,30] considered the anomalous transport of solvents in polymers of finite sizes and solved the partial differential equation for the anomalous transport of solvents.

For a polymer plate with a thickness of 2ℓ and the planar area being much larger than the lateral area, the concentration distribution of methanol at any instant time of t during the

uptake for the anomalous transport of solvents in the polymer plate can be found as[30]

$$C(x,t) = C_0\left\{1 - 2e^{\left(\frac{\nu}{2D}\right)x}\sum_{n=1}^{\infty}\frac{\lambda_n \sin\left(\lambda_n\frac{x}{\ell}\right)}{\beta_n^2\left(1+\frac{2D}{\nu\ell}\cos^2\lambda_n\right)}e^{-\beta_n^2 Dt/\ell^2}\right\}$$

$$\text{for } 0 < x < \ell \tag{1}$$

and

$$C(x,t) = C_0\left\{1 - 2e^{(\nu/2D)(2\ell-x)}\sum_{n=1}^{\infty}\frac{\lambda_n \sin\left(\lambda_n\frac{2\ell-x}{\ell}\right)}{\beta_n^2\left(1+\frac{2D}{\nu\ell}\cos^2\lambda_n\right)}e^{-\beta_n^2 Dt/\ell^2}\right\}$$

$$\text{for } \ell < x < 2\ell \tag{2}$$

with

$$\lambda_n = \frac{-\nu\ell}{2D}\tan\lambda_n \text{ and } \beta_n^2 = \frac{\nu^2\ell^2}{4D^2} + \lambda_n^2 \tag{3}$$

Here, C_0 is the constant solvent concentration at the interfaces between the plate and the solvent ($x = 0$ and $x = 2\ell$), D and ν are the diffusion coefficient for the Case I transport and the velocity for the Case II transport during the methanol absorption, respectively, and λ_n ($n = 1, 2, \ldots$) are the positive roots of the first equation in eqn (3). Integrating eqn (1) and (2) yields the amount of methanol, M, absorbed in the PMMA slab over an immersion time t as

$$\frac{M}{M_\infty} = 1 - 2\sum_{n=1}^{\infty}\frac{\lambda_n^2\left(1 - 2\cos\lambda_n e^{\nu\ell/2D}\right)}{\beta_n^4\left(1+\frac{2D}{\nu\ell}\cos^2\lambda_n\right)}e^{-\beta_n^2 Dt/\ell^2} \tag{4}$$

where $M_\infty(=2\ell C_0)$ is the equilibrium amount of methanol per unit area absorbed in the slab as the immersion time approaches infinity.

Using eqn (4) and the geometrical dimensions of the PMMA–MWCNT plates, one can curve-fit the experimental data presented in Fig. 5 and Fig. S1–S10 in the ESI.† The fitting curves are shown in Fig. 5 with the fitting parameters of D and ν being shown in Fig. 6 and 7, respectively. It is evident that eqn (4) can describe the absorption behavior of methanol in the PMMA–MWCNT plates. The transport behavior of methanol in the PMMA–MWCNT plates with and without UV irradiation follows the anomalous transport.

As discussed above, parameter D is the diffusion coefficient for Case I transport. It is known that the diffusion of solvents is a thermal activation process, and the temperature dependence of the mobility (diffusivity) can be described by the Arrhenius relation. Fig. 6 shows the temperature dependence of the diffusion coefficient, D, for the diffusion of methanol in the PMMA–MWCNT plates with and without UV irradiation. It is evident that the temperature dependence of the diffusion coefficients for a given weight percentage of MWCNTs and UV dose can be described by an exponential function of $(RT)^{-1}$

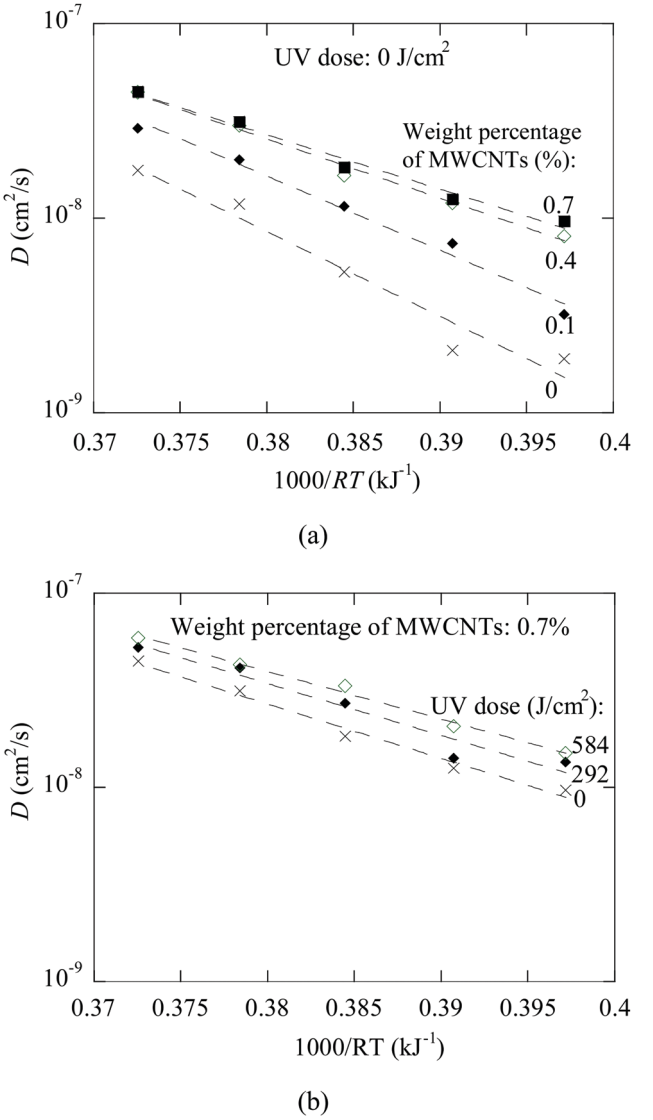

Fig. 6 Temperature dependence of the diffusion coefficient, D, for the methanol transport in the PMMA–MWCNT plates; (a) without UV irradiation for different weight percentages of MWCNTs, and (b) with UV irradiation for the weight percentage of 0.7% MWCNTs.

with R being the gas constant, *i.e.* the Arrhenius relation. Using the Arrhenius relation to curve-fit the experimental data for the diffusion coefficient, one obtains the activation energy for the diffusion of methanol in the PMMA–MWCNT plates.

Table 3 lists the activation energies, E_D and E_ν, of D and ν for the PMMA–MWCNT plates with different weight percentages of MWCNTs, which were irradiated with different UV doses. The addition of MWCNTs in the PMMA–MWCNT plates without UV irradiation leads to the decrease of the activation energy, and has no significant effect on the UV irradiated PMMA–MWCNT plates. UV irradiation leads to the decrease of the activation energy of the rate process controlling Case I transport in the PMMA–MWCNT plates. Such behavior can be attributed to chain scission induced by UV irradiation and the formation of an interfacial region between MWCNTs and the PMMA matrix.

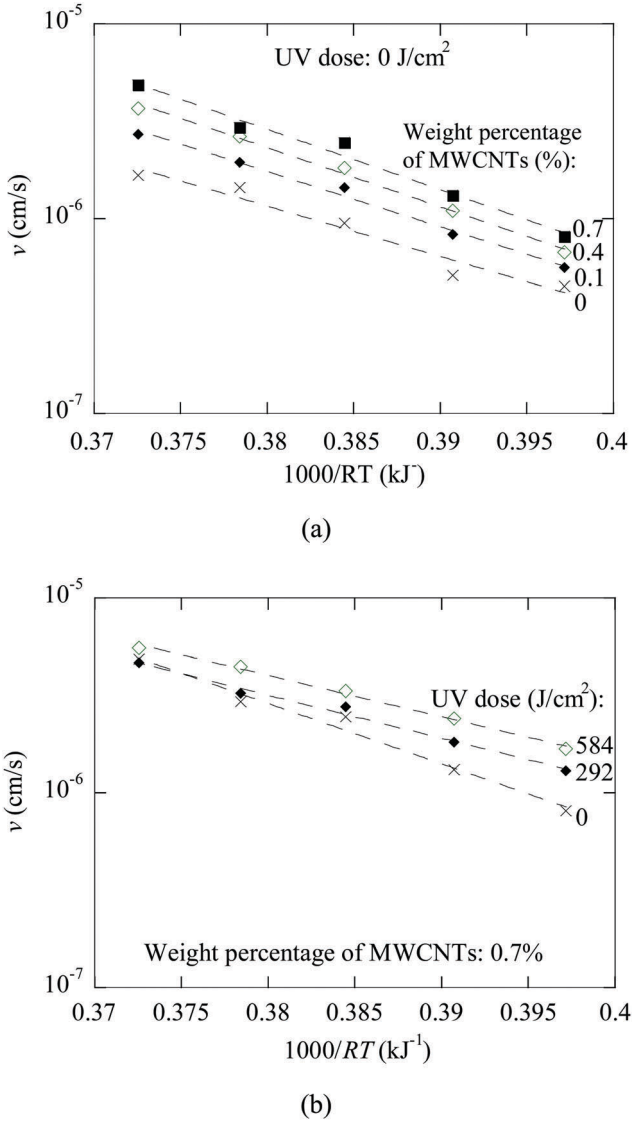

Fig. 7 Temperature dependence of the velocity, v, for Case II transport in the PMMA–MWCNT plates; (a) without UV irradiation for different weight percentages of MWCNTs, and (b) with UV irradiation for the weight percentage of 0.7% MWCNTs.

Table 3 Activation energies, E_D and E_v, of D and v for the PMMA–MWCNT plates with different weight percentages of MWCNTs and different UV doses

	Dose (J cm^{-2})					
	E_D (kJ mol^{-1})			E_v (kJ mol^{-1})		
Wt%	0	291.87	583.74	0	291.87	583.74
0	100.57	83.71	72.74	59.71	47.86	45.65
0.1	88.23	58.72	54.82	65.43	59.12	48.93
0.4	70.28	62.76	53.61	70.03	59.36	51.10
0.7	64.54	61.60	56.36	71.44	50.97	45.25

The UV-induced chain scission reduces the nominal molecular weight, resulting in the decrease of the resistance to the motion of polymer chains and the interaction between polymer chains which cause the decrease of the energy barrier (activation energy) for Case I transport in the UV-irradiated PMMA–MWCNT plates. This trend is qualitatively in accord with the observation by Dole *et al.*,[32] who found that the apparent activation energy increases with the increase of molecular weight for diffusion in a broad range of polymers (polyolefins, polystyrene, polyamide, PVC, PET, PVDC, [ethylene vinyl alcohol copolymer], polyacrylonitrile and [ethylene vinyl acetate copolymer]).

In addition, the hollow structure of MWCNTs provides a fast path through MWCNTs for the methanol transport in the PMMA–MWCNT plates, which likely have smaller energy barriers for the methanol transport than PMMA. The apparent activation energies of the PMMA–MWCNT plates are thus smaller than that of PMMA with the same irradiation dose of UV light.

It is known that the velocity v for Case II transport is associated with the stress relaxation of polymer chains during solvent transport in polymers. The stress relaxation of polymer chains is temperature-dependent. Fig. 7 shows the temperature dependence of the velocity, v, for Case II transport in the PMMA–MWCNT plates with and without UV irradiation. According to Fig. 7a, the larger the weight percentage of MWCNTs in a PMMA–MWCNT plate, the larger the velocity at the same temperature without UV irradiation. This result suggests that the addition of MWCNTs in PMMA enhances Case II transport since the interaction between MWCNTs and polymer chains generally increases the resistance to the migration of polymer chains. The slower stress relaxation of polymer chains corresponds to faster Case II transport. From Fig. 7b, one notes that a PMMA–MWCNT plate irradiated with UV light of a higher dose generally has a larger velocity for Case II transport than a PMMA–MWCNT plate irradiated with UV light of a smaller dose for the same weight percentage of MWCNTs. Such behavior is associated with UV irradiation, which enhances the interaction between MWCNTs and polymer chains (or the stress relaxation of polymer chains becomes difficult) and reduces the resistance to Case II transport.

Similar to the diffusion coefficient, D, the temperature dependence of the velocity can be described by an exponential function of $(RT)^{-1}$, *i.e.* the Arrhenius relation. The stress relaxation of polymer chains during methanol transport in PMMA is a thermal activation process, involving the migration of methanol molecules and polymer chains. Note that stress relaxation also occurs in the interfacial region between MWCNTs and PMMA, which likely has an effect on the movement of both methanol molecules and polymer chains. Using the Arrhenius relation to curve-fit the experimental data for the velocity, one obtains the activation energy associated with Case II transport in the PMMA–MWCNT plates.

Table 3 also lists the variation of the activation energy associated with the velocity with the weight percentage of MWCNTs for the PMMA–MWCNT plates with different UV doses. In contrast to the variation of the activation energy associated with the diffusion coefficient, the activation energy associated with the velocity increases with the increase of the weight percentage of MWCNTs for the PMMA–MWCNTs without UV irradiation. Without UV irradiation, the MWCNTs increase the energy barrier to the stress relaxation of polymer chains due to the interaction

between MWCNTs and polymer chains and become a dominant factor in controlling the stress relaxation. There is no observable trend on the effect of the weight percentage of MWCNTs on the UV-irradiated PMMA–MWCNT plates. Similar to the effect of UV-irradiation on the activation energy associated with the diffusion coefficient, the activation energy associated with the velocity decreases with the increase of the UV dose, suggesting that UV irradiation plays a more important role than MWCNTs in controlling the stress relaxation due to the UV-induced chain scission.

In general, the amount of methanol absorbed in a polymer during immersion is dependent on Case I and Case II transport of methanol in the polymer. As discussed above, both the diffusion coefficient for Case I transport and the velocity for Case II transport are temperature-dependent, following the Arrhenius relation. It is expected that the solvent solubility in the polymer is also temperature dependent, which is similar to vacancies in crystalline metals and alloys. Defining the equilibrium swelling ratio (ESR) as the equilibrium mass of absorbed methanol in a UV-irradiated PMMA–MWCNT plate at a temperature divided by the mass of the specimen before being immersed in methanol, one can use the results shown in Fig. 5 and Fig. S1–S10 in the ESI† to calculate the ESR for the UV-irradiated PMMA–MWCNT plates immersed in methanol at different temperatures. Fig. 8 shows the temperature dependence of the ESR for the methanol transport in the UV-irradiated PMMA–MWCNT plates. It is evident that the ESR increases with the increase of the immersion temperature, independent of the weight percentage of MWCNTs and the UV dose. According to Fig. 8b, the higher the UV dose, the higher the ESR for the PMMA–MWCNT plates immersed at the same temperature. UV irradiation enhances the absorption of methanol. This result suggests that methanol may involve in the chain propagation and chain termination of the free-radical reaction scheme between MWCNTs and PMMA.

In general, the absorption of methanol in the UV-irradiated PMMA–MWCNT plates is an endothermic process. The temperature dependence of the ESR can be described by the van't Hoff equation as

$$\mathrm{ESR} = (\mathrm{ESR})_0 \mathrm{e}^{-\Delta H/RT} \quad (5)$$

where $(\mathrm{ESR})_0$ is a pre-exponential factor and ΔH is the heat of mixing for the absorption process. Using eqn (5) to fit the experimental shown in Fig. 8 and Fig. S11 in the ESI,† one finds the heat of mixing, ΔH. Fig. 8 also includes the fitting curves. It is evident that eqn (5) can be used to describe the temperature dependence of ESR for the absorption of methanol in the UV-irradiated PMMA–MWCNT plates.

Table 4 lists the heat of mixing for the PMMA–MWCNT plates with different weight percentages of MWCNTs and different UV doses. The heat of mixing is positive, implying that the mass transport is an endothermic process. The PMMA–MWCNT plates without UV irradiation have the highest heat of mixing. More energy is needed for the same amount of methanol to be absorbed in the PMMA–MWCNT plates without UV irradiation than that in the case of the PMMA–MWCNTs irradiated with UV light.

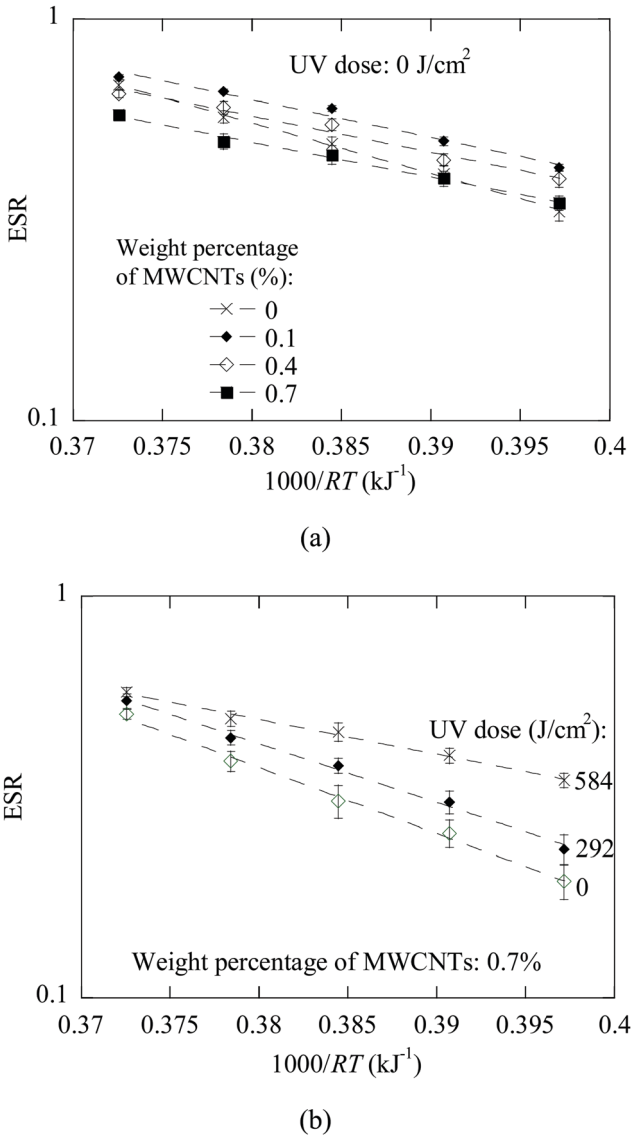

Fig. 8 Temperature dependence of the ESR for the diffusion of methanol in the PMMA–MWCNT plates; (a) without UV irradiation for different weight percentages of MWCNTs, and (b) with UV irradiation for the weight percentage of 0.7% MWCNTs.

Table 4 Heat of mixing, ΔH (kJ mol^{-1}), of methanol for the PMMA–MWCNT composites of different weight percentages of MWCNT subjected to UV doses of 0, 291.87 and 583.74 J cm^{-2}

	Dose (J cm^{-2})		
Wt%	0 (kJ mol^{-1})	291.87 (kJ mol^{-1})	583.74 (kJ mol^{-1})
0	12.61	13.58	13.92
0.1	9.41	9.89	10.19
0.4	8.84	11.88	15.25
0.7	8.79	14.64	16.67

4. Summary

In summary, the PMMA–MWCNT composites have been prepared. The effects of UV irradiation and MWCNTs on the surface morphology, chemical structures, and absorption

of methanol have been studied. The summary of the results is as follows.

(1) UV irradiation has led to the formation of a dense, entangled PMMA–MWCNT layer on the surface of the PMMA–MWCNT plates. Without MWCNTs in PMMA, UV irradiation causes the increase of the surface roughness. The surface roughness of the PMMA–MWCNT composites with UV irradiation decreases with the increase of the weight fraction of MWCNTs.

(2) Photo-induced degradation of PMMA occurs, which leads to the release of MMA to the environment, and photo-assisted interaction between MWCNTs and polymer chains during UV light irradiation. The D–G band ratio increases with the increase of the weight fraction of MWCNTs, and all the three PMMA–MWCNT composites have larger D–G band ratios than the as-received MWCNTs.

(3) Both UV irradiation and the addition of MWCNTs in PMMA enhance the transport of methanol.

(4) The activation energies for Case I and Case II transport decrease with the increase of the UV dose for the PMMA–MWCNT plates with the same weight percentage of MWCNTs. Without UV irradiation, the activation energy for Case I transport decreases with the increase of the weight percentage of MWCNTs, and the activation energy for Case II transport increases with the increase of the weight percentage of MWCNTs.

(5) The PMMA–MWCNT plates without UV irradiation have the highest heat of mixing.

Acknowledgements

SL is grateful for the financial support from the Ministry of Science and Technology, Taiwan. FY is grateful for the financial support from the National Science of Foundation, USA, through Grant No. CMMI-1634540, monitored by Dr Khershed Cooper.

References

1 S. Iijima, Helical microtubules of graphitic carbon, *Nature*, 1991, **354**(6348), 56–58.
2 V. Mittal, *Polymer Nanotubes Nanocomposites: Synthesis*, Properties and Applications, John Wiley & Sons, 2014.
3 R. H. Baughman, A. A. Zakhidov and W. A. de Heer, Carbon nanotubes – the route toward applications, *Science*, 2002, **297**(5582), 787–792.
4 J. Wang, *et al.*, Carbon nanotube fiber microelectrodes, *J. Am. Chem. Soc.*, 2003, **125**(48), 14706–14707.
5 R. H. Baughman, *et al.*, Carbon nanotube actuators, *Science*, 1999, **284**(5418), 1340–1344.
6 P.-J. Cottinet, *et al.*, Electromechanical actuation of bucky-paper actuator: material properties and performance relationships, *Phys. Lett. A*, 2012, **376**(12), 1132–1136.
7 G. Bristow and W. Watson, Cohesive energy densities of polymers. Part 1. – Cohesive energy densities of rubbers by swelling measurements, *Trans. Faraday Soc.*, 1958, **54**, 1731–1741.
8 P. J. Flory, Statistical mechanics of swelling of network structures, *J. Chem. Phys.*, 1950, **18**(1), 108–111.
9 R. Toomey, D. Freidank and J. Rühe, Swelling behavior of thin, surface-attached polymer networks, *Macromolecules*, 2004, **37**(3), 882–887.
10 J. M. Zielinski and J. Duda, Predicting polymer/solvent diffusion coefficients using free-volume theory, *AIChE J.*, 1992, **38**(3), 405–415.
11 A.-S. Michardière, *et al.*, Carbon Nanotube Microfiber Actuators with Reduced Stress Relaxation, *J. Phys. Chem. C*, 2016, **120**(12), 6851–6858.
12 T. Mirfakhrai, *et al.*, Carbon nanotube yarn actuators: an electrochemical impedance model, *J. Electrochem. Soc.*, 2009, **156**(6), K97–K103.
13 T. Mirfakhrai, *et al.*, Electrochemical actuation of carbon nanotube yarns, *Smart Mater. Struct.*, 2007, **16**(2), S243.
14 K. Shah, *et al.*, Development and characterization of polyethylene glycol–carbon nanotube hydrogel composite, *J. Mater. Chem. B*, 2015, **3**(40), 7950–7962.
15 J. Abraham, *et al.*, Transport characteristics of organic solvents through carbon nanotube filled styrene butadiene rubber nanocomposites: the influence of rubber–filler interaction, the degree of reinforcement and morphology, *Phys. Chem. Chem. Phys.*, 2015, **17**(17), 11217–11228.
16 O. Starkova, *et al.*, Water transport in epoxy/MWCNT composites, *Eur. Polym. J.*, 2013, **49**(8), 2138–2148.
17 M. T. Kim, *et al.*, Influence of seawater absorption on the vibration damping characteristics and fracture behaviors of basalt/CNT/epoxy multiscale composites, *Composites, Part B*, 2014, **63**, 61–66.
18 J. C. Yu, *et al.*, A MWCNT/Polyisoprene Composite Reinforced by an Effective Load Transfer Reflected in the Extent of Polymer Coating, *Macromolecules*, 2012, **45**(6), 2841–2849.
19 J. Yip, *et al.*, Tunable carbon nanotube ionic polymer actuators that are operable in dry conditions, *Sens. Actuators, B*, 2012, **162**(1), 76–81.
20 T. Villmow, *et al.*, Polymer/carbon nanotube composites for liquid sensing: model for electrical response characteristics, *Polymer*, 2011, **52**(10), 2276–2285.
21 C. Decker, Kinetic study and new applications of UV radiation curing, *Macromol. Rapid Commun.*, 2002, **23**(18), 1067–1093.
22 A. Faucitano, *et al.*, Photo-oxidation and stabilization of polymers, *Trends Polym. Sci.*, 1996, **4**(3), 92–98.
23 R. S. McLean and B. B. Sauer, Tapping-mode AFM studies using phase detection for resolution of nanophases in segmented polyurethanes and other block copolymers, *Macromolecules*, 1997, **30**(26), 8314–8317.
24 M. J. Cadena, *et al.*, Sub-surface imaging of carbon nanotube–polymer composites using dynamic AFM methods, *Nanotechnology*, 2013, **24**(13), 135706.
25 M. A. Pantoja-Castro, *et al.*, Synthesis and investigation of PMMA films with homogeneously dispersed multiwalled carbon nanotubes, *Mater. Chem. Phys.*, 2013, **140**, 458–464.
26 N. S. Kalospiros, *et al.*, Analysis of anomalous diffusion and relaxation in solid polymers, *Ind. Eng. Chem. Res.*, 1991, **30**(5), 851–864.

27 T. Alfrey, E. Gurnee and W. Lloyd, Diffusion in glassy polymers, *Journal of Polymer Science Part C: Polymer Symposia*, Wiley Online Library, 1966.
28 T. Wang, T. Kwei and H. Frisch, Diffusion in glassy polymers. III, *J. Polym. Sci., Part A-2*, 1969, **7**(12), 2019–2028.
29 J. P. Harmon, S. Lee and J. Li, Anisotropic methanol transport in PMMA after mechanical deformation, *Polymer*, 1988, **29**(7), 1221–1226.
30 J. P. Harmon, S. Lee and J. Li, Methanol transport in PMMA: The effect of mechanical deformation, *J. Polym. Sci., Part A: Polym. Chem.*, 1987, **25**(12), 3215–3229.
31 D. Chiang, *et al.*, Methanol desorption in poly(methyl methacrylate) with stress distributions, *J. Mater. Res.*, 2014, **29**(18), 2162.
32 P. Dole, *et al.*, Typical diffusion behaviour in packaging polymers–application to functional barriers, *Food Addit. Contam.*, 2006, **23**(2), 202–211.